

Abstract

Theoretical condensed matter research is plagued by a fundamental issue of complexity. The sheer amount of degrees of freedom in a material on any technologically relevant scale is overwhelming (e.g. $\sim 10^{23}$ electrons per cm^3), and makes it impossible to describe the quantum mechanical wavefunction exactly.

The Hamiltonian plays a central role in the description of crystals, the subject of this thesis. It can be decomposed into various parts, and their interactions. Depending on the physics under scrutiny it then often suffices to solve only one of those parts. This can be either because the energy scales and associated timescales that govern the constituents are very different, or because the interactions between them are small. One example, often put into practice, is the separation of electronic and phononic (lattice) degrees of freedom, leading to the well-known Born-Oppenheimer approximation, decoupling their respective motion. Another is the often neglected spin-orbit coupling, due to the tiny prefactor associated with its relativistic origin.

Solving these subproblems then allows for progress to be made in understanding the physics that govern them. However, there will inevitably be systems for which this interaction is not small and leads to fascinating new physics that manifestly depends on both subsystems combined. In this thesis we focus on these cases and how they arise in functional materials, with the occasional eye towards applications in technology.

The reason why these cross-order couplings can be interesting for technological applications, is that often one of the orders is more robust with respect to perturbations, and therefore more long-lived, but also harder to control efficiently. By exploiting the cross-order coupling in certain materials, one could potentially control the long lived order by applying perturbations to the more easily controllable order.

In giant Rashba effect systems, the coupling between spin and ferroelectric order leads to a linear spin-splitting of the band structure, whose sign depends on the orientation of the ferroelectric polarization. We show that, rather than the relativistic Rashba effect, a combination of electrostatics and atomic spin-orbit coupling lies at the origin of the large splitting.

The coupling between magnetism and ferroelectricity in multiferroic GdMn_2O_5 leads to a never before observed four-state hysteresis loop for the ferroelectric polarization, which depends on the magnitude, angle and history of the applied magnetic field. As we will show, this four-state hysteresis loop is accompanied by a full 360° rotation of spins in the material, which resembles the crankshaft of a car, converting the linear back-and-forth motion of the magnetic field into a rotational motion of the spins.

In a thin film of elemental Chromium, the ultrafast dynamics of a spin

density wave, coupled to a slower varying charge density wave, allows for a high degree of control of the latter through excitations of the former. This allows us to predict the sequence of optical pulses to be applied to the material in order to follow closely an enveloping signal function.

And finally, the coupling between ferroelectricity and strain in BaTiO₃ leads to a softening at purely ferroelectric domain walls, allowing for some mechanical control of the position of this wall.

We utilize both theoretical and computational tools to understand the nature of these interactions, how they lead to cross-order coupling in these materials, and how this then translates into the experimentally observed behavior.

Chapter 1

Coupling between spin and strain density waves

1.1 Introduction

In the previously discussed situations, the coupling between the orders was relatively static. In the case of GeTe the polarization influenced the sign of the spin splitting, but was assumed static in the description. While there was an element of a time evolution in the GdMn₂O₅ it was assumed that the magnetic field varied at a slow enough rate such that both the polarization as the magnetic order were always at equilibrium. Similarly, while the experiments performed on BaTiO₃ where dependent on a resonance frequency, this was assumed to not influence the material itself and thus the description was again static. New physics arise, however, when two orders with different timescales for their dynamics are coupled. This is the case in the material we study here, Chromium, an itinerant antiferromagnetic metal [**Kulikov1984**, **Fawcett1988**]. It is the hallmark example of a material where a spin density wave (SDW) develops due to local repulsive interactions of the electron gas, combined with a nesting of the fermi surface. Due to magnetostriction, this spin density wave then causes a periodic lattice displacement (PLD) which decreases the bondlengths between the spins that have large magnitude. The SDW is formed by electrons and thus thermalizes on very quick timescales when a perturbation is applied [**Nicholson2016**]. The coupled PLD, however, denotes the movement of atoms and thus has much slower dynamics. With ultrafast pump-probe experiments that have a below picosecond resolution, these PLD dynamics can be studied and, more importantly, controlled very precisely through excitation of the much faster responding SDW. Among other things, this allows for the suppression of the intermediate state and reproducing adiabatic transitions on much faster timescales which is termed “shortcuts to adiabaticity” in quantum technology [**Torrontegui2013**, **Deffner2014**, **Zhou2017**]. This also allows to apply a specific set of pulses in order for the PLD oscillation to follow a particular envelope function, as will be shown theoretically below.

1.2 Experimental methods

Before focusing on the theoretical description of the coupling between the SDW and PLD, we take a look at the experimental techniques employed by A. Singer's group and the results that we are seeking to reproduce. A thin film (28 nm) of Cr was used, supporting around seven periods of the SDW with a Néel temperature T_N of 290 K, slightly lower than in the bulk where $T_N \approx 308$ K. The film was illuminated by two sequential 40 fs optical pulses at times τ_1 and τ_2 , heating up the electronic subsystem and the SDW which is a part of it. Due to magnetostriction, this SDW is coupled with a PLD which is probed through the Bragg peaks by an x-ray free-electron laser (XFEL)[**Singer2015**]. The scattering intensity of the Bragg peak is directly proportional to the magnitude of the PLD, offering both phase and amplitude information of the PLD oscillation that occurs when the SDW is (partially) melted by the optical pulses. The high resolution ultrafast measurements that the XFEL enables (fs timescales), allows to follow the evolution of the PLD in time. The acoustic phonon associated with the PLD oscillation has a wavevector normal to the material surface and an oscillation period of approximately 450 fs. The heat exchange rate between the lattice (or bath) and the electrons is quite high, leading to a thermalization between the two subsystems within a picosecond after heating. Even though some heat is deposited in the system, and the heat capacity is not infinite, the final temperature stays below the Néel temperature leading to a recovery of the SDW and eventually the PLD, as can be seen by the non-zero oscillation equilibrium at the end of the measurements in Fig. ???. Further thermalization of the Cr lattice to the substrate occurs on the nanosecond timescale, out of the scope of our measurements. Due to the slight increase in temperature of the system (around 45 K), this equilibrium amplitude of the PLD is slightly lower after the pulses, compared with before. The damping time of the PLD is around 3 ps. It is important to realize that the SDW order is not directly accessible through these kinds of measurements, so we are effectively studying the effect of exciting one order parameter through the reaction of the other by the coupling between them.

The most interesting observation is that by changing the timing of the second pulse τ_2 , the dynamics of the PLD can be controlled to a high degree. In Fig. ??(b-c) it can be seen that the oscillation amplitude in the first one is almost completely destroyed by the second pulse, whereas in panel c it is increased slightly. Panel a of the same figure shows a more complete visualization of this effect, where the horizontal bands with low amplitude signify the destructive interference and those with high amplitude the constructive situation.

The maximum PLD amplitude that is reached in the experiments, after the second pulse is 150% of the original amplitude. This is significantly higher than the excitation amplitudes associated with the conventional displacive excitation mechanism, where the ratio is about one [**Singer2015, Zeiger1992**]. When the second pulse arrives before the SDW had time to cool down, the maximum oscillation amplitude is lowered as can be seen from the horizontal band around $\tau_2 - \tau_1 = 0$ ps in Fig. ??(a). As will be further discussed below, this signifies that the SDW momentarily exceeds T_N , and additional heating does not contribute to a larger excitation of the PLD phonon.

Experiments performed at higher fluence, i.e. such that the SDW gets heated above T_N from a single pulse, show that the second pulse does not impact

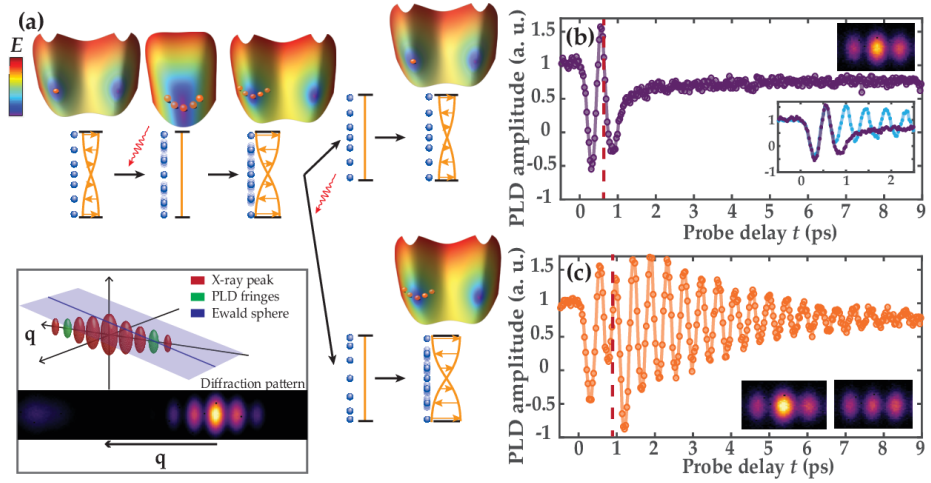


Figure 1.1: **Controlled enhancement and destruction of the excited state.** (a) A laser pulse excites the system by destroying the magnetic order; a second pulse either excites the released phonon further or stops the excitation. Schematic energy surfaces show the PLD state as the orange point. Inset: x-ray scattering from periodic atomic displacement is detected on a fringe of the main peak from the crystalline film. (b-c) Amplitude of the PLD in two extreme control cases. Solid lines are experimental data (empty circles) - connected. The dashed red line marks the time of second pulse arrival. (b) $\tau_2 - \tau_1 = 620$ fs, (c) $\tau_2 - \tau_1 = 845$ fs. Insets show the Laue fringe with the satellite peak at maximum and minimum PLD values.

the oscillation of the PLD, as can be seen from Fig. ??(c). If control is the goal, it is thus important that the SDW is kept below T_N . Moreover, the SDW order parameter varies the most with temperature when it is close to the critical point, increasing the pulse efficiency. XFELs also allow for higher peak selectivity (narrow and intense satellite Bragg peaks), such that it allows for measurements performed on thin films even deposited on thick substrates, as was the case in the experiments performed by A. Singer et.al. This absence of topological defects is confirmed by the absence of a widening of the satellite peak associated with the PLD, as compared with the peaks of the material itself. [not sure about this, I actually don't understand what they are talking about in the paper either].

1.3 Theory

[some explanation of Peierls instabilities etc, the things that cause the SDW in the first place?]

As was already aluded to, we can describe the effect of the photon pulses by considering two subsystems with two temperatures. The first is the electronic subsystem, that thermalizes on a 100 fs timescale, as was shown by high-resolution ARPES measurements [Nicholson2016], and can thus be considered to be always thermal on the picosecond timescales that we are interested in, allowing us to assign a temperature to it. The SDW is formed by electronic states

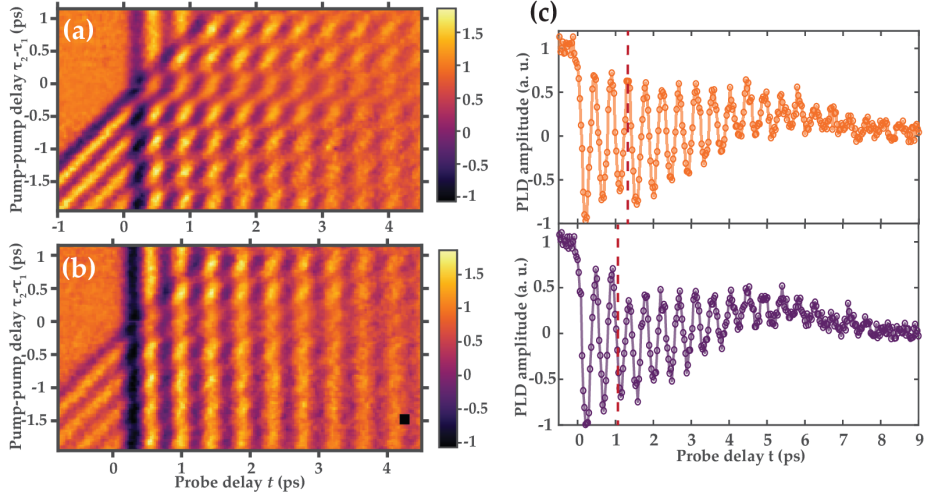


Figure 1.2: Experimental maps of the excited state depending on probe and pump delay. (a) Map of the PLD amplitude before and after excitation by two pulses with a fluence of 1.45 mJ/cm^2 . (b) Same as (a) but with the second pulse twice less intense than the first. (c) Magnitude of the PLD in “enhancement” and “suppression” conditions at laser pulse fluence of 9.5 mJ/cm^2 for the first and 4.7 mJ/cm^2 for the second. The dashed line marks the arrival time of the second pulse, $\tau_2 - \tau_1 = 1295 \text{ fs}$ for the top panel and 1065 fs for the bottom.

and thus belongs to the electronic subsystem [Nicholson2016], with the same temperature T_L . The second subsystem is the lattice (phonon modes excluding the mode associated with the PLD) which we denote as the bath which is always assumed to be thermal, with temperature T_b . After the electronic system absorbs the heat from the pulses, it will exchange heat with this bath, cooling it down within one picosecond. This process can be described by the so-called two temperature model:

$$\begin{aligned} C_L \dot{T}_L &= -k(T_L(t) - T_b(t)) + Q_p h(t) \\ C_b \dot{T}_b &= -k(T_b(t) - T_L(t)), \end{aligned} \quad (1.1)$$

with k the heat transfer rate, C_L and C_b the heat capacities of the electronic degrees of freedom and bath, respectively. The dots signify time derivatives. As one could expect, we find that the heat capacity of the bath is larger than that of the electronic system by an order of magnitude[ref]. Finally, the heat injected by the pulses is modelled by a gaussian $Q_p h(t) = A e^{-\frac{(t-t_0)^2}{\tau^2}}$, with A the strength, τ the duration and t_0 the time delay.

The changes to T_L through heating and subsequent cooling affects the amplitude SDW order parameter L and indirectly the one describing the PLD y , as described by a Landau-type theory [Khomskii2010]. These order parameters are related to the Fourier component of the SDW with wavevector q , i.e. $L = S_q$, and to the acoustic phonon amplitude $y = u_{2q}$. The phonon mode is the second harmonic ($2q$) of the SDW because the magnetostriction acts on the magnitude of the spins, and not the phase, so that during one period of

the SDW oscillation two periods of the PLD occur. This leads to the following expression for the total free energy:

$$F(L, y, T_L) = \frac{\alpha}{2}(T_L - T_c)L^2 + \frac{\beta}{4}L^4 - gL^2y + \frac{\omega_0}{2}y^2 + \frac{b}{4}y^4, \quad (1.2)$$

where L , y and T_L are the time dependent variables. The double well potential that leads to the SDW phase transition is characterised by α and β , with the temperature of the SDW given by T_L and critical temperature T_c below which the SDW order sets in. The magnetostrictive coupling between the two order parameters is described by term with γ . Only even orders of L appear in the free energy, since the energy is time reversal even, but L is time reversal odd. The PLD order parameter y has a zero equilibrium value without the presence or interaction with L , since it is not the primary order parameter. The fourth order term $\frac{b}{4}y^4$ is only included to provide a better fit to some of the anisotropic features of observed by the experiment, not to bound the energy potential in terms of y , as would be required if y was the primary order parameter with a negative second order term, like in the case of L . It is the interaction with the primary order parameter L that provides the “force” to move y up in its own potential, leading to the nonzero equilibrium value. While this sounds trivial, this concept is the key to understanding the observed physics.

The time evolution of the system can be described using the Langrangian:

$$\mathcal{L}(L, y, \dot{L}, \dot{y}, t) = \frac{m_L \dot{L}(t)^2}{2} + \frac{m_y \dot{y}(t)^2}{2} - F(L, y, t), \quad (1.3)$$

with associated Euler-Lagrange equations:

$$\begin{aligned} \frac{\partial \mathcal{L}}{\partial L} - \frac{d}{dt} \frac{\partial \mathcal{L}}{\partial \dot{L}} &= \gamma_y \dot{L} \\ \frac{\partial \mathcal{L}}{\partial y} - \frac{d}{dt} \frac{\partial \mathcal{L}}{\partial \dot{y}} &= \gamma_L \dot{y} \end{aligned} \quad (1.4)$$

where the γ denote the damping parameters for both order parameters. Substituting Eq. ?? leads to

$$\begin{aligned} m_L \ddot{L} &= -\alpha(T_L - T_c)L - \beta L^3 - \gamma_L \dot{L} + 2gLy \\ m_y \ddot{y} &= -\omega_0^2 y - by^3 - \gamma_y \dot{y} + gL^2. \end{aligned} \quad (1.5)$$

These equations, together with Eqs. ?? describing the temperature evolution of the SDW (T_L) under influence of the optical pulses, fully describe the dynamics that are experimentally observed. One obvious remark can be made here, in that to be completely exact, the energy dissipated through the damping terms in Eq. ?? should be absorbed into the bath and thus influence T_b . However, the case can be made that since this is only a single mode, its contribution to the heating of the bath will be negligible compared with the one due to the thermalization of all the electronic degrees of freedom.

1.4 Methods

To solve the time evolution of L and y through the differential equations in Eqs. ?? we used the numerical integration methods implemented in the DifferentialEquations.jl package [[rackauckas2017differentialequations](#)]. More

specifically the Tsit5 algorithm was used, which has adaptive timestepping to capture the sharp pulses. Originally the dynamics were fully solved both for L and y , but it was found during the fitting process that the dynamics of L are significantly faster than those of y , i.e. both the “mass” of the SDW order is orders of magnitude smaller than that for y parameter, and the parameters describing the Landau free energy potential are orders of magnitude larger. This all leads to the SDW almost perfectly tracking its instantaneous minimum on the timescales that are of interest. Solving dynamics with significantly different timescales is in general hard from the numerical point of view, and while there are other ways around this, we opted to take $m_L = 0$ and use the instantaneous minimum in the equation describing the dynamics of y . This minimum is found by minimizing the Landau free energy in Eq. ?? for a given y and T_L in terms of L such that $\frac{\partial F}{\partial L} = 0$, leading to:

$$L(t) = \pm \sqrt{\frac{-\alpha(T_L - T_c) + 2gy}{\beta}}. \quad (1.6)$$

The starting temperature of the bath was fixed at 115 K, and T_c was observed to be at 290 K, consistent with previous observations that in general the Néel temperature of a thin film is lower than that of the bulk material (bulk Cr has a Néel temperature of ≈ 310 K). Most parameters of the model described above were not known a priori and thus had to be fitted to the experimental measurements. To aid with the fitting, judicious starting values could be chosen for some parameters. For example, it was known that the pulse width τ was under 100 fs, the oscillation frequency of the PLD $\omega_0 \approx 14$ or equivalently a period of around 450 fs. It was also known that in general the second pulse had a fluency of around 80% that of the first, and we also chose the initial heat capacities for the bath and electronic degrees of freedom to have a ratio $\frac{c_b}{c_L}$ close to 7, which was known from previous experiments [citation].

For each set of trial parameters, the time evolution of the system was solved on an interval of -2 ps to 8 ps, where the lower bound is chosen so that the numerical integration starts from a completely equilibrium initial condition. This is needed because when the sharp pulse arrives around 0 ps, some energy already enters the system slightly before 0 ps due to the gaussian shape. The error of the solution \hat{x} w.r.t. the experimental measurements x is then the mean square sum $err = \sum_{i=1}^n \frac{(x_i - \hat{x}_i)^2}{n}$, where i denote the measurement points. The numerical optimization was done through the Optim package, where it was found that the Nelder Mead simplex algorithm [citation needed] works best for this very non-linear problem.

1.5 Results

The experimental results we use as a basis to fit our model to are shown in Fig. ???. In the numerical model, we found in earlier trials that the dynamics of the SDW order parameter L is orders of magnitude faster than the ones from the PLD y , as expected. This can also be seen from Fig. ?? since the energy potential is a lot flatter for y than for L , leading to a slower time evolution. This difference in dynamics makes it extremely hard to solve the differential equations numerically, we therefore assumed that at each timestep the L order parameter

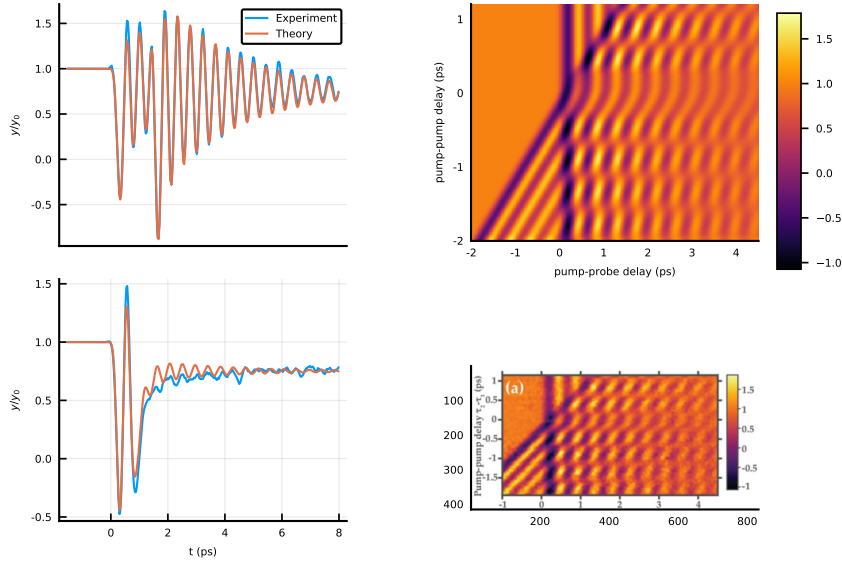


Figure 1.3: Comparison of theoretical fit vs Experiment. (a-b) Two examples of fits to constructive (a) and destructive (b) experiments. (c-d) Comparison of the theoretically generated heatmap (c) with the experimental heatmap (d).

is in equilibrium in its instantaneous energy potential. This is equivalent to the limit of the mass m_L in Eq. ?? going to zero. The value of L at a given T_L and y can be found by minimizing the Landau free energy ??

$$L_0 = \pm \sqrt{\frac{\alpha(T_L - T_c) + 2gy}{\beta}}. \quad (1.7)$$

This eliminates to evaluate Eq. ??, instead using Eq. ?? to evaluate L in the partial differential equation for the evolution of y .

We then took eleven representative experiments, which can be thought of as horizontal slices of Fig. ??(a), in order to fit the model parameters to get the best total fit accross all datasets. The parameters are

$$\alpha = 6039, \beta = 7.97 \times 10^7, g = 0.52, \gamma_L = 25.0, \quad (1.8)$$

$$\omega_0 = 14.1, b = 3.38 \times 10^8, \gamma_y = 0.76, \quad (1.9)$$

$$f = 64.43, c_b = 3.58, c_L = 0.36, k = 1.29, \tau = 0.074 \quad (1.10)$$

The results of this fitting procedure is shown in Fig. ??, showing an excellent agreement between the theory and experiment.

To get a deeper understanding of the underlying effect, we look at the evolution of the free energy surfaces for both order parameters, as shown in Fig. ???. The characteristic double well potential for $L \neq 0$ equilibrium is clearly visible, and as expected, when the pulses hit and T_L increases in the term $\alpha(T_L - T_c)L^2$ of Eq. ??, we see that the potential flattens causing the the minimum of L to very quickly change, as discussed above. This in turn causes the single-well

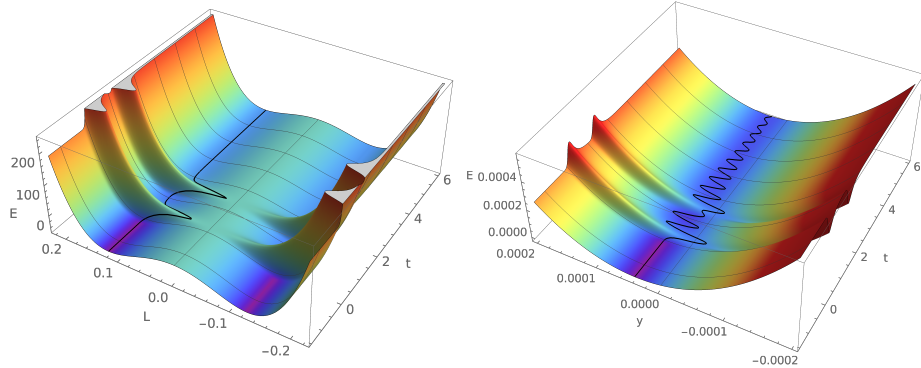


Figure 1.4: Time evolution of the energy surfaces of the order parameters.

potential of y to shift as quickly. The dynamics of y is orders of magnitude slower than that of L and due to this instant shift of the energy surface, it will cause an oscillation of y . While the temperature T_L decreases again, L and the minimum of the y potential shift back towards the original equilibrium position. The oscillation of y remains for a relatively long time while this shift is occurring since the damping is not that big (of the order of 4ps). It then becomes clear that if the second pulse can repeat this mechanism while the oscillation of y is still there, it can be increased or decreased depending on the timing. Having this understanding, let's investigate what the ideal way to excite y is.

First of all, when the system is relatively close to the phase transition of L , a small increase of temperature causes a large change in the value of L as shown through Eq. ??, and thus causes a large the shift of the potential for y . It is then important to keep this initial shift of the potential for y in place until y crosses the minimum, converting as much potential energy into "kinetic" energy. This requires L to be heated slightly above the PT, which leads to the largest possible shift of the potential of y , and the additional temperature of L above T_c , together with the non-infinite cooling rate, allows y to gain the maximum kinetic energy. Since only the size of L matters for the potential surface of y , it can only cause a shift in one direction, meaning that, similar to someone pushing a swing, the ideal intervals for the subsequent pulses are close to multiples of the period of y , if the goal is maximum oscillation amplitude. The amount of periods depends on the cooling rate of L , this influences how much T_L can cool back down within one period and thus the size of the maximum shift, since this depends on distance of T_L from T_c , and the damping of y since that is the main source of kinetic energy loss. Taking these understandings into consideration, a high degree of control of the oscillation of y can be achieved through the intensity, amount and timing of a pulse train applied to the material. To demonstrate this, we went one step further and utilized the fitted model to simulate what pulse train has to be applied to the material in order for the oscillation maxima to follow a given envelope signal. To limit the dimensionality of the manifold of possible solutions, we performed the following ruleset:

- Only one fluence can be used per pulse
- Pulses are grouped in sets per period of oscillation

- The first pulse group only has a single pulse, applied 20 fs after the first non zero value of the envelope function, this determines the fluence of each pulse
- The maximum allowed pulses per group is fixed
- The groups are then fitted sequentially, since the later pulses don't influence the oscillation caused by the earlier ones
- If the function is seen to increase during a period, the pulses will be initiated close to the ideal boost location, and if a decrease is required, close to the ideal brake location

Adhering to these rules, we tested this procedure on different envelope functions, showcased in Fig. ???. One assumption made here was that the heat capacity of the bath c_b was increased to infinity, this is done because with the increase of temperature of the bath, the equilibrium position of L changes and leads to a general downwards slope of the oscillation of y as see from panel (a-b) of Fig. ??.

Having fit the model, we can go one step further and try to fit the PLD oscillation to an arbitrary signal shape. To this end we use the fitted model, and predict the timing of a fixed fluence pulse train that will result in the required shape. The results are shown in Fig. ???. This showcases that with an arbitrary pulse train we can achieve indirect, but optimal control of the PLD order parameter.

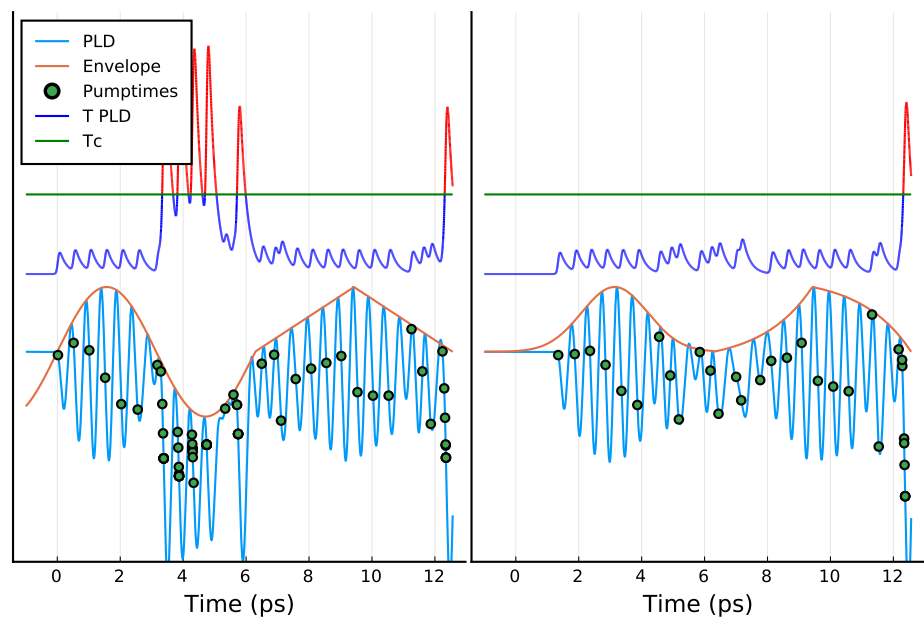


Figure 1.5: Two examples of optimal control. (a) Shows a reproduction of a sinusoidal envelope function, (b) shows the result for more complicated envelope, with an the absolute value of a sinusoidal followed by a half a period of a sawtooth function. The pulse train is highlighted by the purple dots, and the evolution of the temperature of the SDW is given by the orange plot.